ISME

Iranian Journal of Mechanical Engineering
The Iranian Society of Mechanical Engineers
Research Paper
DOI: 10.30506/JMEE.2021.132091.1240

Coupled Thermoelasticity of FGM Truncated Conical Shells

H. Eliasi *
M.Sc. Student

M. Bateni †
PhD Student

M. R. Eslami ‡
Professor

This article presents the coupled thermoelasticity of a truncated functionally graded conical shell under thermal shock load. The classical coupled thermoelasticity theory is employed to set the partial differential equations of motion of the conical shell. The shell governing equations are based on the first-order shear deformation shell theory that accounts for the transverse shear strains and rotations. The solution is obtained by transforming the governing equations into the Laplace domain and using the Galerkin finite element method in the Laplace domain to calculate the displacement components. The physical displacement components in real time domain are obtained by the numerical inversion of the Laplace transform. Temperature distribution is assumed to be linear across the shell thickness. Radial displacement, axial stress, axial force, and temperature versus time are calculated and the effect of relaxation time and power law index are examined. Comparison indicates that an increase in the radial vibration amplitude and a decrease of vibration frequency occur when changing the material from ceramic to metal. The results are validated with the known data in the literature.

Keywords: Coupled thermoelasticity, Conical shell, Functionally graded materials

1 Introduction

The coupled thermoelasticity refers to the interaction of elastic and thermal deformations in a continuum. The solution of this class of problems requires simultaneous consideration of the equations of motion and the energy equation. Due to this nature, assumption of dynamic coupled thermoelasticity requires a deep physical and mathematical understanding to properly model and solve the governing equations.

One of the topics in thermoelasticity is the coupled thermoelastic analysis of structural members such as beams, plates, and shells. Structural members in various industries may be subjected to severe thermal loads in a short period of time. In such circumstances, the coupled thermoelastic assumption is necessary to evaluate the dynamic thermo-mechanical fields through the structural members.

* M.Sc. Student, Department of Mechanical Engineering, Amirkabir University of Technology, Tehran, Iran, h.elyasi.m@gmail.com
† PhD Student, Department of Mechanical Engineering, Amirkabir University of Technology, Tehran, Iran, masoud.bateni@aut.ac.ir
‡ Corresponding author, Department of Mechanical Engineering, Amirkabir University of Technology, Tehran, Iran, eslami@aut.ac.ir
Received:2020/08/03, Accepted: 2021/01/23

Researches are conducted on the coupled thermoelastic analysis of structural members. Ignaczak and Nowacki [1] have addressed such an analysis. They presented the coupled thermoelastic formulations for dynamical analysis of plates under non-steady temperature distributions. Jones [2] presented an investigation on the coupled thermoelastic behavior of beams. This work contains the EulerBernoulli and Timoshenko beam hypotheses, and presents formulations for beams with different thermal and mechanical boundary conditions. Researches on coupled thermoelasticity of beams are extended to geometrically nonlinear analysis [3], and beams made of functionally graded materials (FGMs) [4]. Among the early studies on the coupled thermoelastic analysis of thin plates, the work done by Inan [5] could be mentioned. This work implemented an analytical approach and investigated the free vibration as well as general solution of the associated equations of motion of thin elastic plates for thermo-mechanically coupled conditions. Chang and Wan [6] present a Galerkin-based investigation on the thermo-mechanically coupled large amplitude vibrations of thin elastic plates. This work presents some results on damping aspect of coupled thermoelastic analysis, and a comparison between the coupled and un-coupled results. Trajkovski and Čukić [7] presented the dynamic coupled thermoelastic behavior of circular plates under a surface thermal shock load. This work uses a solution based on the integral transforms which has the capability for exact implementation of boundary conditions. For investigation on the effect of thermo-mechanical coupling on the nonlinear dynamics of orthotropic plates, Yeh [8] used a Galerkin-based solution method. This work is presented for plates with simply supported boundary conditions, and plate's behavior is considered to be governed by the classical plate theory. The results of this work mainly show the effects of material and geometrical characteristics of plates, stemming from the thermo-mechanical coupling and orthotropicity of plate's material on the amplitude decaying of their vibrational motion. Research is also conducted to investigate the dynamic coupled thermoelastic behavior of plates made of functionally graded materrials. In this regard, works done by Akbarzadeh et al. [9] and Jafarinezhad and Eslami [10], respectively, present dynamic thermoelastic analysis on behavior of rectangular and annular plates subjected to lateral thermal shocks. The leading work on the analysis of the dynamic thermoelastic response of shell structures belongs to McQuillen and Brull [11]. The numerical results of this work address the behavior of infinite-length cylindrical shells subjected to suddenly applied and rotating longitudinal lines of heat flux. Eslami et al. [12], by means of the Galerkin finite element procedure, investigated the dynamic thermoelastic response of long cylindrical shells subjected to thermal and mechanical shocks. Using the Ritz finite element method, Chang and Shyong [13] presented an investigation on the vibrational behavior of laminated cylindrical shell panels subjected to a surface thermal shock. Through the numerical results of this work, effects of themo-mechanical coupling, boundary conditions, ply angles, and radius of curvature on dynamic thermoelastic response of laminated cylindrical shell panels are studied. Eslami et al. [14] investigated the dynamic coupled thermoelastic behavior for shells of revolution based on the Flügge second-order shell theory. This work uses the Galerkin finite element method for solving the governing equations and exhibits the effect of normal stress and strain on the response of shells to thermal and mechanical shocks. The dynamic coupled thermoelastic response has also been studied for cylindrical shells made of FGMs, see the work by Bahtui and Eslami [15]. This work utilizes a second-order shear-deformable shell model as the kinematical idealization and a Galerkin trans-finite element method as the solution procedure. Kraus [16] has presented the dynamic thermoelastic analysis of spherical shells. However, the work is formulated in the context of un-coupled thermoelasticity theory. Amiri et al. [17] have presented the dynamic coupled thermoelastic response of thin spherical shells. Coupled thermoelasticity of thin conical shells under thermal shock load is considered by Soltani et al [18]. The shell material is considered to be made of

homogeneous/isotropic material, temperature distribution across the shell thickness is assumed to be a quadratic function of the thickness variable and the Galerkin finite element method is employed to solve the coupled equations. The coupled equations are directly solved in the space and time domain using the Newmark method. Coupled thermoelasticity of rotating truncated conical shells based on the Lord-Shulman model is presented by Heydarpour and Aghdam [19]. While the title of the paper is conical shells, but the authors consider a thick shell segment and use the theory of elasticity and the equations of motion along the axial and radial directions. The differential quadrature method is used to solve the governing equations. Since the theory of elasticity is used to model the problem, the temperature and stress wave fronts should be detected in the corresponding figures. No clear discussion for the wave fronts is given in the numerical result section of the article. This conclusion is the critical issue and the authors should have provided a brief discussion on the interaction of the speed of rotation and the magnitudes and locations of the temperature and stress wave fronts.

The present work deals with the dynamic coupled thermoelastic response of truncated FGM conical shells to suddenly applied thermal shocks. The work is formulated based on a first-order shear-deformable shell model. The shell is considered to obey Hooke's law for their mechanical material properties and to accept infinitesimal strains under the applied load conditions. The classical dynamic coupled energy equation is used to obtain the temperature distribution through the shells. The temperature field in shell's thickness direction is approximated to vary linearly. Based on the governing equations, a flexural coupled thermoelastic element is derived. Also, the effects of shell slenderness and thermal edge conditions on the dynamic coupled thermoelastic response of thin conical hells to lateral thermal shock loads are investigated.

2 Analysis

A truncated conical FGM shell with radii R_i and R_o, thickness h, and the half apex angle β, as shown in Figure (1), is considered. The functionally graded shell is made of metal and ceramic, where the material properties continuously change in the thickness direction as a function of location. The material properties such as Youngs modules $E(z)$, coefficient of thermal expansion $\alpha(z)$, coefficient of heat conduction $K(z)$, specific heat $C(z)$, and the mass density $\rho(z)$ are described across the shell thickness, where z is the shell thickness coordinate between $-h/2$ and $h/2$, positive outward. The volume fraction of constituent materials are denoted by

$$f_m = \frac{V_m}{V_m + V_c} \qquad \mathrm{f}_c = \frac{V_c}{V_m + V_c} \tag{1}$$

where f_m and f_c are the volume fractions of metal and ceramic of FGM, respectively, and satisfy the following equation

$$f_m + f_c = 1 \tag{2}$$

The effective material properties of functionally graded materials may be expressed as

$$F_{cf}(z) = F_m f_m + F_c f_c \tag{3}$$

where F_m and F_c are the persistent material properties of each phase. The volume fraction is assumed to follow a power law function as

$$i \geq 0, \mathrm{f}_m = \left(\frac{2z + h}{2h}\right)^i, \mathrm{f}_c = 1 - f_m \tag{4}$$

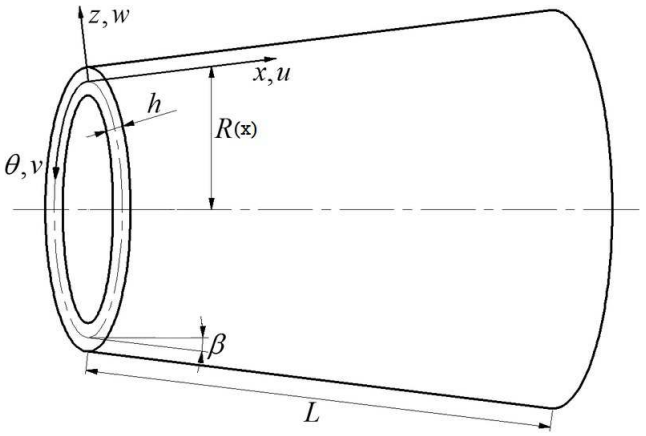

Figure 1 Truncated conical shell with displacement fields.

where i is the power law index and represents the material variation through the shell thickness. When value of i equals to zero, it represents a fully metal and when infinity it represents a fully ceramic shell. It is assumed that Poissons ratio is constant across the shell thickness due to its negligible variation for the constituents.

2.1 Strain-displacement relations

Structure in this problem is a functionally graded truncated conical shell. The conical coordinates (x, θ, z) are considered along the axial, circumferential, and normal to shell surface directions. The displacement components based on the first order approximation are represented as

$$\begin{aligned} u(x,\theta,z) &= u_0(x,\theta) + z\psi_x(x,\theta) \\ v(x,\theta,z) &= v_0(x,\theta) + z\psi_\theta(x,\theta) \\ w(x,\theta,z) &= w_0(x,\theta) \end{aligned} \tag{5}$$

where u_0, v_0, and w_0 represent the components of displacement vector in the middle plane of the shell at a point along the x, θ, and z-directions, respectively.

The strain-displacement relations for the conical shell based on first order shear deformation theory are given as

$$\begin{aligned} \varepsilon_x &= \frac{\partial u_\circ}{\partial x} + z\frac{\partial \psi_x}{\partial x} \\ \varepsilon_\theta &= \frac{1}{1+\frac{z}{R_v}}\left[\frac{1}{R}\frac{\partial v_\circ}{\partial \theta} + \frac{u_\circ}{R}\sin\beta + \frac{w_\circ}{R}\cos\beta + \frac{z}{R}\left(\frac{\partial \psi_\theta}{\partial \theta} + \psi_x \sin\beta\right)\right] \\ \gamma_{\theta z} &= \frac{1}{1+\frac{z}{R_v}}\left(\frac{1}{R}\frac{\partial w_\circ}{\partial \theta} + \psi_\theta - \frac{v_\circ}{R}\cos\beta\right) \\ \gamma_{xz} &= \frac{\partial w_\circ}{\partial x} + \psi_x \\ \gamma_{x\theta} &= \frac{\partial v_\circ}{\partial x} + z\frac{\partial \psi_\theta}{\partial x} + (\frac{1}{1+\frac{z}{R_v}})\left[\frac{1}{R}\frac{\partial u_\circ}{\partial \theta} - \frac{v_\circ}{R}\sin\beta + \frac{z}{R}(\frac{\partial \psi_x}{\partial \theta} - \psi_\theta \sin\beta)\right] \end{aligned} \tag{6}$$

where in these equations $R = R(x)$ and $R_v = R\cos\beta$.

2.2 Stress-strain relations

The stress - strain relations for a functionally graded shell based on the assumed displacement model, including the shear deformations, are

$$\left\{\begin{array}{c}\sigma_x\\ \sigma_\theta\\ \tau_{x\theta}\\ \tau_{xz}\\ \tau_{\theta z}\end{array}\right\}=\frac{E(z)}{1-\upsilon^2}\left[\begin{array}{ccccc}1 & \upsilon & 0 & 0 & 0\\ \upsilon & 1 & 0 & 0 & 0\\ 0 & 0 & \frac{1-\upsilon}{2} & 0 & 0\\ 0 & 0 & 0 & \frac{1-\upsilon}{2} & 0\\ 0 & 0 & 0 & 0 & \frac{1-\upsilon}{2}\end{array}\right]\left\{\begin{array}{c}\varepsilon_x-\alpha(z)(\Delta T)\\ \varepsilon_\theta-\alpha(z)(\Delta T)\\ \gamma_{x\theta}\\ \gamma_{xz}\\ \gamma_{\theta z}\end{array}\right\} \tag{7}$$

The force and moment resultants from the first order shell theory are

$$\begin{aligned}&< N_{xx}, N_{\theta\theta}, N_{\theta x}, N_{x\theta}, Q_{xx}, Q_{\theta\theta} >=\int_{-h/2}^{h/2}< \sigma_{xx}, \sigma_{\theta\theta}, \tau_{\theta x}, \tau_{x\theta}, \tau_{xz}, \tau_{\theta z} >dz\\ &< M_{xx}, M_{\theta\theta}, M_{\theta x}, M_{x\theta} >=\int_{-h/2}^{h/2}< \sigma_{xx}, \sigma_{\theta\theta}, \tau_{\theta x}, \tau_{x\theta} >zdz\end{aligned} \tag{8}$$

2.3 Equations of motion

The following equations are obtained by the Hamilton principle, in conical coordinates, including the shear deformations [16]

$$\begin{aligned}&N_{xx,x}.R(x)+N_{\theta x,\theta}+(N_{xx}-N_{\theta\theta})\sin\beta=R(x)(I_\circ\ddot{u}_\circ+I_1\ddot{\psi}_x)\\ &N_{x\theta,x}.R(x)+N_{\theta\theta,\theta}+(N_{x\theta}+N_{\theta x})\sin\beta+Q_\theta.\sin\beta=R(x)(I_\circ\ddot{v}_\circ+I_1\ddot{\psi}_\theta)\\ &Q_{x,x}.R(x)+Q_{\theta,\theta}+Q_x.\sin\beta-N_{\theta\theta}.\cos\beta=R(x)(q+I_\circ\ddot{w}_\circ)\\ &M_{xx}.sin\beta+M_{xx,x}.R(x)+M_{\theta x,\theta}-M_{\theta\theta}.\sin\beta-R(x)Q_x=R(x)(I_1\ddot{u}_\circ+I_2\ddot{\psi}_x)\\ &M_{x\theta,x}.R(x)+M_{\theta\theta,\theta}+(M_{x\theta}+M_{\theta x})\sin\beta-R(x)Q_\theta=R(x)(I_1\ddot{v}_\circ+I_2\ddot{\psi}_\theta)\end{aligned} \tag{9}$$

where

$$\begin{aligned}&\int_{-h/2}^{h/2}\rho(z)dz=I_0\\ &\int_{-h/2}^{h/2}\rho(z)zdz=I_1\\ &\int_{-h/2}^{h/2}\rho(z)z^2dz=I_2\end{aligned} \tag{10}$$

For the axisymmetric loading conditions, Eqs. (9) reduce to

$$\begin{aligned}&N_{xx,x}+(N_{xx}-N_{\theta\theta})\frac{\sin\beta}{R}=I_\circ\ddot{u}_\circ+I_1\ddot{\psi}_x\\ &Q_{x,x}+Q_x.\frac{\sin\beta}{R}-N_{\theta\theta}\frac{\cos\beta}{R}=q+I_\circ\ddot{w}_\circ\\ &M_{xx,x}+(M_{xx}-M_{\theta\theta})\frac{\sin\beta}{R}-Q_x=I_1\ddot{u}_\circ+I_2\ddot{\psi}_x\end{aligned} \tag{11}$$

Temperature distribution across the shell thickness may be assumed to be linear, as

$$T(x,\theta,z,t)-T_a=T_0(x,\theta,t)+zT_1(x,\theta,t) \tag{12}$$

where T_a is the reference temperature and T_1 and T_2 are the unknown functions to be obtained. Substituting Eqs. (6) into Eqs. (7) and using Eqs. (10) and (12) and finally substituting the resulting equations into the equations of motion (11), the equations of motion are obtained in terms of the displacement components as

$$\begin{aligned}
&(A_{111}\frac{\partial^2}{\partial x^2}+A_{111}\frac{\sin\beta}{R}\frac{\partial}{\partial x}-A_{111}\frac{\sin^2\beta}{R^2}-I_0\frac{\partial^2}{\partial t^2})u_0+(-A'_{111}\frac{\cos\beta}{R}\frac{\partial}{\partial x}\\
&-A_{111}\frac{\sin\beta\cos\beta}{R^2})w_0+(B_{111}\frac{\partial^2}{\partial x^2}+B_{111}\frac{\sin\beta}{R}\frac{\partial}{\partial x}-B_{111}\frac{\sin^2\beta}{R^2}\\
&-I_1\frac{\partial^2}{\partial t^2})\psi_x-(G_{11}\frac{\partial}{\partial x})T_0-(G_{22}\frac{\partial}{\partial x})T_1=0\\
&(-A'_{111}\frac{\cos\beta}{R}\frac{\partial}{\partial x}-A_{111}\frac{\cos\beta\sin\beta}{R^2})u_0+(A''_{111}\frac{\partial^2}{\partial x^2}+A_{111}\frac{\sin\beta}{R}\frac{\partial}{\partial x}\\
&-A_{111}\frac{\cos^2\beta}{R^2}-I_0\frac{\partial}{\partial t^2})w_0+(A''_{111}\frac{\partial}{\partial x}-B'_{111}\frac{\cos\beta}{R}\frac{\partial}{\partial x}+A''_{111}\frac{\sin\beta}{R}\\
&-B_{111}\frac{\cos\beta\sin\beta}{R^2})\psi_x+(G_{11}\frac{\cos\beta}{R})T_0+(G_{22}\frac{\cos\beta}{R})T_1=0\\
&(B_{111}\frac{\partial^2}{\partial x^2}+B_{111}\frac{\sin\beta}{R}\frac{\partial}{\partial x}-B_{111}\frac{\sin^2\beta}{R^2}-I_1\frac{\partial^2}{\partial t^2})u_0+(-B'_{111}\frac{\cos\beta}{R}\frac{\partial}{\partial x}\\
&-B_{111}\frac{\sin\beta\cos\beta}{R^2}-A''_{111}\frac{\partial}{\partial x})w_0+(C_{111}\frac{\partial^2}{\partial x^2}+C_{111}\frac{\sin\beta}{R}\frac{\partial}{\partial x}\\
&-C_{111}\frac{\sin^2\beta}{R^2}-I_2\frac{\partial^2}{\partial t^2}-A''_{111})\psi_x-(G_{22}\frac{\partial}{\partial x})T_0-(G_{33}\frac{\partial}{\partial x})T_1=0
\end{aligned} \tag{13}$$

where $A_{111}, A'_{111}, A''_{111}, B_{111}, B'_{111}, C_{111}, G_{ii}(i=1..3)$ are constants given in the Appendix. Three equations of motion contain five unknown dependent functions u_0, w_0, ψ_x, T_0, and T_1. This means that two more equations are needed to complete the necessary equations and calculate the dependent functions. These two equations are derived by employing the energy equation.

2.4 Energy equation

The first law of thermodynamics for heat conduction equation is assumed for the functionally graded truncated conical shell. The classical theory of coupled thermoelasticity for the FG truncated conical shell is considered as [21]

$$\rho c_\epsilon\dot{T}+\bar{\beta}T_a\dot{\epsilon_{ii}}=(kT_{,i})_{,i} \tag{14}$$

where ρ is the mass density, c_ϵ is the specific heat at constant strain, $\bar{\beta}=\alpha(3\lambda+2\mu)$, T_a is the reference temperature, and k is the heat conduction coefficient. This equation may be written in expanded form for the assumed conditions. We move all parts of the equation to the left side of the equation and call it the residue Re. The resulting residue Re is made orthogonal with

respect to 1 and z. This yields two independent equations for T_0 and T_1, as it is made orthogonal with respect to 1 and z for T_0 and T_1 [11]

$$\int_{-h/2}^{h/2} Re \times dz = 0$$
$$\int_{-h/2}^{h/2} Re \times z dz = 0 \tag{15}$$

Five governing equations, including the equations of motion and the energy equations, must be simultaneously solved to obtain the displacements and temperature functions.

As the thermal boundary conditions, it is considered that the heat flux Q_{in} and Q_{out} are applied on the inside and outside surfaces of the cone

$$k(-h/2)\frac{\partial T}{\partial z}\bigg|_{-\frac{h}{2}} = h_{in}\left(T - T_{\infty}^{in}\right) \quad , \quad z = -\frac{h}{2} \tag{16}$$

$$k(h/2)\frac{\partial T}{\partial z}\bigg|_{\frac{h}{2}} = h_{out}\left(T - T_{\infty}^{out}\right) \quad , \quad z = \frac{h}{2} \tag{17}$$

Using Eqs. (12) and (15) for the linear approximation of temperature distribution across the thickness direction, two energy equations for the conical shell are obtained as

$$\begin{aligned}
&\left[T_a H_1\left(\tfrac{\partial^2}{\partial x \partial t} + \tfrac{\sin\beta}{R}(\tfrac{\partial}{\partial t})\right)\right] u_0 + \left[T_a H_1 \tfrac{\cos\beta}{R}\left(\tfrac{\partial}{\partial t}\right)\right] w_0 \\
&+ \left[T_a H_2\left(\tfrac{\partial^2}{\partial x \partial t} + \tfrac{\sin\beta}{R}(\tfrac{\partial}{\partial t})\right)\right] \psi_x \\
&+ \left[K_1\left(\tfrac{\partial}{\partial t}\right) - J_1 \tfrac{\sin\beta}{R}\tfrac{\partial}{\partial x} - J_1 \tfrac{\partial^2}{\partial x^2}\right] T_0 \\
&+ \left[K_2\left(\tfrac{\partial}{\partial t}\right) - J_2 \tfrac{\sin\beta}{R}\tfrac{\partial}{\partial x} - J_2 \tfrac{\partial^2}{\partial x^2}\right] T_1 \\
&= Q_{out} - Q_{in}
\end{aligned}$$

$$\begin{aligned}
&\left[T_a H_2\left(\tfrac{\partial^2}{\partial x \partial t} + \tfrac{\sin\beta}{R}(\tfrac{\partial}{\partial t})\right)\right] u_0 + \left[T_a H_2 \tfrac{\cos\beta}{R}\left(\tfrac{\partial}{\partial t}\right)\right] w_0 \\
&+ \left[T_a H_3\left(\tfrac{\partial^2}{\partial x \partial t} + \tfrac{\sin\beta}{R}(\tfrac{\partial}{\partial t})\right)\right] \psi_x \\
&+ \left[K_2\left(\tfrac{\partial}{\partial t}\right) - J_2 \tfrac{\sin\beta}{R}\tfrac{\partial}{\partial x} - J_2 \tfrac{\partial^2}{\partial x^2}\right] T_0 \\
&+ \left[K_3\left(\tfrac{\partial}{\partial t}\right) - J_3 \tfrac{\sin\beta}{R}\tfrac{\partial}{\partial x} - J_3 \tfrac{\partial^2}{\partial x^2} + J_1\right] T_1 \\
&= \tfrac{h}{2}(Q_{out} + Q_{in})
\end{aligned} \tag{18}$$

where the constants $H_j, K_j, J_j (j = 1...3)$ are given in the Appendix.

2.5 Numerical solution

Consider a truncated conical shell under axisymmetric thermal shock load. Temperature distribution across the shell thickness is assumed to be linear. Under such assumed conditions

five unknown functions u_0, w_0, ψ, T_0, T_1, as given by Eqs. (13) and (18), appear in the governing equations. These equations are transformed into the dimensionless form by the following dimensionless parameters

$$\begin{array}{lll}
\bar{x} = \frac{x}{\delta} & & \\
\bar{t} = \frac{tC_1}{\delta} & & \\
\Delta\bar{T} = \frac{T-T_a}{T_a} & \bar{T}_0 = \frac{T_0}{T_a} & \bar{T}_1 = \frac{\delta T_1}{T_a} \\
\bar{u}_0 = \frac{(\lambda_m+2\mu_m)u_0}{\delta\gamma_m T_a} & \bar{w}_0 = \frac{(\lambda_m+2\mu_m)w_0}{\delta\gamma_m T_a} & \bar{\psi}_x = \frac{(\lambda_m+2\mu_m)\psi_x}{\gamma_m T_a} \\
\bar{\sigma}_{ij} = \frac{\sigma_{ij}}{\gamma_m T_a} & &
\end{array} \tag{19}$$

where $\gamma_m = E_m\alpha_m$ indicating that γ_m is evaluated for the metal constituent and

$$C_1 = \sqrt{\frac{\lambda_m + 2\mu_m}{\rho_m}}$$

$$\delta = \frac{k_m}{\rho_m c_m C_1}$$

Here, λ and μ are the Lamè constants and the subscript m denotes the material properties of metal constituent. With the assumed dimensionless parameters, the governing equations are transformed into the Laplace domain. Consider the linear shape function for the base element of the dependent functions as

$$\begin{aligned}
\overline{u_0} &= \left\langle \; u_{0i} \quad u_{0j} \; \right\rangle \left\{ \begin{array}{c} N_i \\ N_j \end{array} \right\} \\
\overline{w_0} &= \left\langle \; w_{0i} \quad w_{0j} \; \right\rangle \left\{ \begin{array}{c} N_i \\ N_j \end{array} \right\} \\
\overline{\psi_\theta} &= \left\langle \; \psi_{\theta i} \quad \psi_{\theta j} \; \right\rangle \left\{ \begin{array}{c} N_i \\ N_j \end{array} \right\} \\
\overline{T_0} &= \left\langle \; T_{0i} \quad T_{0j} \; \right\rangle \left\{ \begin{array}{c} N_i \\ N_j \end{array} \right\} \\
\overline{T_1} &= \left\langle \; T_{1i} \quad T_{1j} \; \right\rangle \left\{ \begin{array}{c} N_i \\ N_j \end{array} \right\}
\end{aligned} \tag{20}$$

where $N_i = 1 - \frac{\bar{x}}{l}$ and $N_j = \frac{\bar{x}}{l}$, l being the length of base element (e). Applying the Galerkin method to the system of five Laplace transferred equations and employing the weak formulations, yield

$$\begin{aligned}
&\int_0^l \Big[(-A_{111}\tfrac{\delta}{(\lambda_m+2\mu_m)}\tfrac{\partial N_l}{\partial x}\tfrac{\partial N_m}{\partial x} - A'''_{111}\tfrac{\sin^2\beta}{R^2}\tfrac{\delta}{(\lambda_m+2\mu_m)}N_l N_m \\
&-A'_{111}\tfrac{\sin\beta}{R}\tfrac{\delta}{(\lambda_m+2\mu_m)}\tfrac{\partial N_l}{\partial x}N_m + A'''_{111}\tfrac{\sin\beta}{R}\tfrac{\delta}{(\lambda_m+2\mu_m)}N_l\tfrac{\partial N_m}{\partial x} \\
&-I_0\tfrac{1}{\rho_m\delta}s^2 N_l N_m)\bar{u}_0 + (-A'''_{111}\tfrac{\cos\beta\sin\beta}{R^2}\tfrac{\delta}{(\lambda_m+2\mu_m)}N_l N_m \\
&-A'_{111}\tfrac{\cos\beta}{R}\tfrac{\delta}{(\lambda_m+2\mu_m)}\tfrac{\partial N_l}{\partial x}N_m)\bar{w}_0 + (-B_{111}\tfrac{\delta}{(\lambda_m+2\mu_m)}\tfrac{\partial N_l}{\partial x}\tfrac{\partial N_m}{\partial x} \\
&-B'''_{111}\tfrac{\sin^2\beta}{R^2}\tfrac{\delta}{(\lambda_m+2\mu_m)}N_l N_m - B'_{111}\tfrac{\sin\beta}{R}\tfrac{\delta}{(\lambda_m+2\mu_m)}\tfrac{\partial N_l}{\partial x}N_m \\
&+B'''_{111}\tfrac{\sin\beta}{R}\tfrac{\delta}{(\lambda_m+2\mu_m)}N_l\tfrac{\partial N_m}{\partial x} - I_1\tfrac{1}{\rho_m\delta^2}s^2 N_l N_m)\bar{\psi}_x \\
&+(G_{11}\tfrac{1}{\gamma_m}\tfrac{\partial N_l}{\partial x}N_m)\bar{T}_0 + (G_{22}\tfrac{1}{\gamma_m\delta}\tfrac{\partial N_l}{\partial x}N_m)\bar{T}_1\Big]\,dx = \tfrac{1}{T_a\gamma_m}(-\bar{N}xx.N_l)
\end{aligned}$$

$$
\begin{aligned}
&\int_0^l \Big[(-A_{111}\tfrac{\delta}{(\lambda_m+2\mu_m)}N_l\tfrac{\partial N_m}{\partial x} - A'_{111}\tfrac{\cos\beta\sin\beta}{R^2}\tfrac{\delta}{(\lambda_m+2\mu_m)}N_lN_m)\bar{u}_0\\
&+(A''_{111}\tfrac{\sin\beta}{R}\tfrac{\delta}{(\lambda_m+2\mu_m)}N_l\tfrac{\partial N_m}{\partial x} - A''_{111}\tfrac{\delta}{(\lambda_m+2\mu_m)}\tfrac{\partial N_l}{\partial x}\tfrac{\partial N_m}{\partial x}\\
&-A_{111}\tfrac{\delta}{(\lambda_m+2\mu_m)}\tfrac{\cos^2\beta}{R^2}N_lN_m - I_0\tfrac{1}{\rho_m\delta}s^2N_lN_m)\bar{w}_0\\
&+(-B_{111}\tfrac{\delta}{(\lambda_m+2\mu_m)}\tfrac{\cos\beta}{R}N_l\tfrac{\partial N_m}{\partial x} - B'_{111}\tfrac{\sin\beta\cos\beta}{R^2}\tfrac{\delta}{(\lambda_m+2\mu_m)}N_lN_m\\
&-A''_{111}\tfrac{\delta}{(\lambda_m+2\mu_m)}\tfrac{\partial N_l}{\partial x}N_m + A''_{111}\tfrac{\sin\beta}{R}\tfrac{\delta}{(\lambda_m+2\mu_m)}N_lN_m)\bar{\psi}_x\\
&+(G_{11}\tfrac{\cos\beta}{R}\tfrac{1}{\gamma_m}N_lN_m)\bar{T}_0 + (G_{22}\tfrac{\cos\beta}{R}\tfrac{1}{\gamma_m\delta}N_lN_m)\bar{T}_1\Big]\,dx = \tfrac{1}{T_a\gamma_m}(-\bar{Q}xx.N_l)
\end{aligned}
$$

$$
\begin{aligned}
&\int_0^l \Big[(-B_{111}\tfrac{1}{(\lambda_m+2\mu_m)}\tfrac{\partial N_l}{\partial x}\tfrac{\partial N_m}{\partial x} - B'''_{111}\tfrac{\sin^2\beta}{R^2}\tfrac{1}{(\lambda_m+2\mu_m)}N_lN_m\\
&-B'_{111}\tfrac{\sin\beta}{R}\tfrac{1}{(\lambda_m+2\mu_m)}\tfrac{\partial N_l}{\partial x}N_m + B'''_{111}\tfrac{\sin\beta}{R}\tfrac{1}{(\lambda_m+2\mu_m)}N_l\tfrac{\partial N_m}{\partial x}\\
&-I_1\tfrac{1}{\rho_m\delta}s^2N_lN_m)\bar{u}_0 + (-B'''_{111}\tfrac{\cos\beta\sin\beta}{R^2}\tfrac{1}{(\lambda_m+2\mu_m)}N_lN_m\\
&-B'_{111}\tfrac{\cos\beta}{R}\tfrac{1}{(\lambda_m+2\mu_m)}\tfrac{\partial N_l}{\partial x}N_m - A''_{111}\tfrac{1}{(\lambda_m+2\mu_m)}N_l\tfrac{\partial N_m}{\partial x})\bar{w}_0\\
&+(-C_{111}\tfrac{1}{(\lambda_m+2\mu_m)}\tfrac{\partial N_l}{\partial x}\tfrac{\partial N_m}{\partial\bar{x}} - C'''_{111}\tfrac{\sin^2\beta}{R^2}\tfrac{1}{(\lambda_m+2\mu_m)}N_lN_m\\
&-C'_{111}\tfrac{\sin\beta}{R}\tfrac{1}{(\lambda_m+2\mu_m)}\tfrac{\partial N_l}{\partial x}N_m + C'''_{111}\tfrac{\sin\beta}{R}\tfrac{1}{(\lambda_m+2\mu_m)}N_l\tfrac{\partial N_m}{\partial x}\\
&-I_2\tfrac{1}{\rho_m\delta^2}s^2N_lN_m - A''_{111}\tfrac{1}{(\lambda_m+2\mu_m)}N_lN_m)\bar{\psi}_x + (G_{22}\tfrac{1}{\gamma_m\delta}\tfrac{\partial N_l}{\partial x}N_m)\bar{T}_0\\
&+(G_{33}\tfrac{1}{\gamma_m\delta^2}\tfrac{\partial N_l}{\partial x}N_m\bar{T}_1)\Big]\,dx = \tfrac{1}{\delta\ T_a\gamma_m}(-\bar{M}xx.N_l)
\end{aligned}
$$

$$
\begin{aligned}
&\int_0^l \Big\{\Big[H_1\Big(\tfrac{1}{\gamma_mT_a}(sN_l\tfrac{\partial N_m}{\partial x}) + \tfrac{\sin\beta}{R}\tfrac{1}{\gamma_mT_a}(sN_lN_m)\Big)\Big]\bar{u}_0\\
&+\Big[H_1\tfrac{\cos\beta}{R}\tfrac{1}{\gamma_mT_a}\,(sN_lN_m)\Big]\bar{w}_0\\
&+\Big[H_2\Big(\tfrac{1}{\delta\gamma_mT_a}(sN_l\tfrac{\partial N_m}{\partial x}) + \tfrac{\sin\beta}{R}\tfrac{1}{\delta\gamma_mT_a}(sN_lN_m)\Big)\Big]\bar{\psi}_x\\
&+(K_1\tfrac{(\lambda_m+2\mu_m)T_a}{\delta(\gamma_mT_a)^2}\,(sN_lN_m) - J_1\tfrac{(\lambda_m+2\mu_m)T_a}{(\gamma_mT_a)^2C_1}\tfrac{\sin\beta}{R}N_l\tfrac{\partial N_m}{\partial x}\\
&-J_1\tfrac{(\lambda_m+2\mu_m)T_a}{(\gamma_mT_a)^2C_1}\tfrac{\partial N_l}{\partial x}\tfrac{\partial N_m}{\partial x})\bar{T}_0 + (K_2\tfrac{(\lambda_m+2\mu_m)T_a}{\delta^2(\gamma_mT_a)^2}\,(sN_lN_m)\\
&-J_2\tfrac{(\lambda_m+2\mu_m)T_a}{\delta(\gamma_mT_a)^2C_1}\tfrac{\sin\beta}{R}N_l\tfrac{\partial N_m}{\partial x} - J_2\tfrac{(\lambda_m+2\mu_m)T_a}{\delta(\gamma_mT_a)^2C_1}\tfrac{\partial N_l}{\partial x}\tfrac{\partial N_m}{\partial x})\bar{T}_1\Big\}\,dx\\
&=\int_0^l(-\bar{Q}_{in}+\bar{Q}_{out})N_l dx
\end{aligned}
$$

$$
\begin{aligned}
&\int_0^l \Big\{\Big[H_2\Big(\tfrac{1}{\delta\gamma_mT_a}(sN_l\tfrac{\partial N_m}{\partial x}) + \tfrac{\sin\beta}{R}\tfrac{1}{\delta\gamma_mT_a}(sN_lN_m)\Big)\Big]\bar{u}_0\\
&+\Big[H_2\tfrac{\cos\beta}{R}\tfrac{1}{\delta\gamma_mT_a}\,(sN_lN_m)\Big]\bar{w}_0\\
&+\Big[H_3\Big(\tfrac{1}{\delta^2\gamma_mT_a}(sN_l\tfrac{\partial N_m}{\partial x}) + \tfrac{\sin\beta}{R}\tfrac{1}{\delta^2\gamma_mT_a}(sN_lN_m)\Big)\Big]\bar{\psi}_x\\
&+(K_2\tfrac{(\lambda_m+2\mu_m)T_a}{\delta^2(\gamma_mT_a)^2}\,(sN_lN_m) - J_2\tfrac{(\lambda_m+2\mu_m)T_a}{\delta(\gamma_mT_a)^2C_1}\tfrac{\sin\beta}{R}N_l\tfrac{\partial N_m}{\partial x}\\
&-J_2\tfrac{(\lambda_m+2\mu_m)T_a}{\delta(\gamma_mT_a)^2C_1}\tfrac{\partial N_l}{\partial x}\tfrac{\partial N_m}{\partial x})\bar{T}_0 + (K_3\tfrac{(\lambda_m+2\mu_m)T_a}{\delta^3(\gamma_mT_a)^2}\,(sN_lN_m)\\
&-J_3\tfrac{(\lambda_m+2\mu_m)T_a}{\delta^2(\gamma_mT_a)^2C_1}\tfrac{\sin\beta}{R}N_l\tfrac{\partial N_m}{\partial x} - J_3\tfrac{(\lambda_m+2\mu_m)T_a}{\delta^2(\gamma_mT_a)^2C_1}\tfrac{\partial N_l}{\partial x}\tfrac{\partial N_m}{\partial x}\\
&+J_2\tfrac{(\lambda_m+2\mu_m)T_a}{\delta^3(\gamma_mT_a)^2C_1}N_lN_m)\bar{T}_1\Big\}\,dx = \int_0^l\tfrac{h}{2\delta^2}(\bar{Q}_{in}+\bar{Q}_{out})N_l dx
\end{aligned}
\tag{21}
$$

where s is the Laplace variable. Here, Q_{in} and Q_{out} are the inner and outer non-dimension applied heat flux. Set of Eqs. (21) are assembled for all the finite elements of the solution domain and the final equation in the Laplace domain is given as

$$[K(s)]\{X\} = \{F(s)\} \tag{22}$$

Table 1 Material properties of functionally graded constituent materials.

Metal	Ceramic
$E_m = 66.2$ Gpa	$E_c = 117$ Gpa
α_m = 10.3 $\times 10^{-6}(1/K)$	$\alpha_c = 7.11 \times 10^{-6}(1/K)$
ρ_m = 4.41 $\times 10^3(kg/m^3)$	$\rho_c = 5.6 \times 10^3(kg/m^3)$
$k_m = 18.1(W/mK)$	$k_c = 2.036(W/mK)$
$c_m = 808.3$ (J/kg.K)	$c_c = 615.6$ (J/kg.K)
ν = 0.321	ν = 0.333

where $[K(s)]$ is the global stiffness matrix, $\{F(s)\}$ is the global force matrix, and $\{X\}$ is the global unknown matrix in form of the non-dimensional displacement components defined by Eqs. (20) in the Laplace transform domain. Note that since the time domain is transformed into the s-domain (Laplace), the mass, capacitance, and stiffness element matrices are compressed into one matrix, called the global stiffness matrix $[K(s)]$. The finite element equilibrium equation (22) is solved in the Laplace domain and the inverse Laplace transform to bering the solution into the real time domain t is handled using the numerical inversion of Laplace transform. For the solution of Eq. (22) and transformation into the real time domain t, the method developed by Brancik [25] for fast numerical inversion of Laplace transforms is developed in Matlab language environment.

2.6 Results and discussion

Consider a simply supported functionally graded conical shell under the inside impulsive thermal shock. The ratio of thickness to small radius is assumed to be 0.1 and ratio of small radius to length of conical shell is assumed to be 0.1. The functionally graded shell is assumed to be made of combination of metal (Ti6Al4V) and ceramic (ZrO2), at the initial temperature 298.15K, with the material properties shown in Table 1.

The shell is ceramic-rich at the inside and metal-rich at the outside surfaces, respectively. Temperature field across the shell thickness is assumed to be of linear type. Thermal shock is of impulsive type and is applied to the inside surface. The equation of thermal shock is

$$\bar{Q}_1 = 50\bar{t}e^{-10\bar{t}} \tag{23}$$

The boundary conditions at the ends of the shell are assumed to be thermally insulated. For the FG shell, the power law index is assumed to be $i = 0$, 5, and $i = \infty$. Figure 2 shows the lateral deflection of the shell middle length versus time for different values of the power law index. Since the modulus of elasticity of ceramic is larger than metal, as the power law index i increases, the normal frequency which is directly proportional to the modulus of elasticity increases. When the power law index i increases, the displacement amplitude decreases too. Figure 3 shows the temperature of the shell middle length versus time. This figure shows that for pure ceramic shell ($i = \infty$), temperature distribution becomes higher, as the ceramic conductivity is lower compared to metal. The reason is that lower thermal conductivity of ceramics increases the temperature of the structure under applied thermal shock load. Figure 4 shows the lateral deflection of the shell middle length versus time for different cone angles. This figure shows that the lateral displacement increases and its frequency decreases as the cone angle increases. When the cone angle is increased, the shell approaches to an annular plate and when the cone angle is decreased it approaches to cylindrical shell. The conical shells with larger

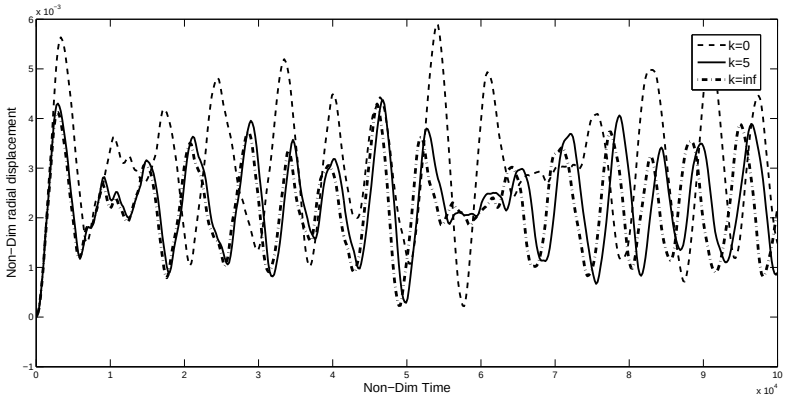

Figure 2 Radial displacement of middle length of the shell versus time for different power law indices.

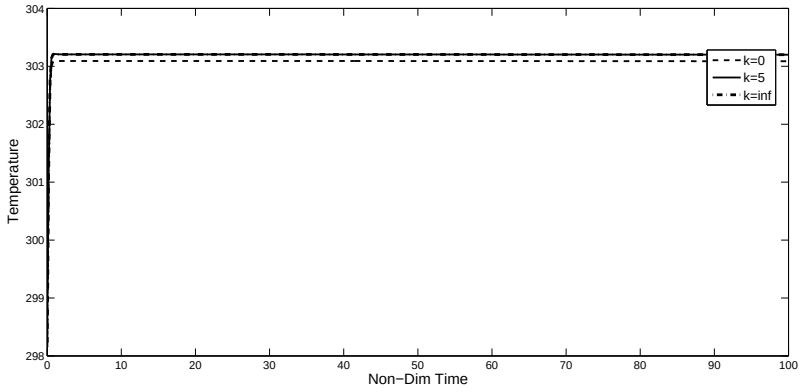

Figure 3 Temperature of middle length and mid-plane of the shell versus time for different power law indices.

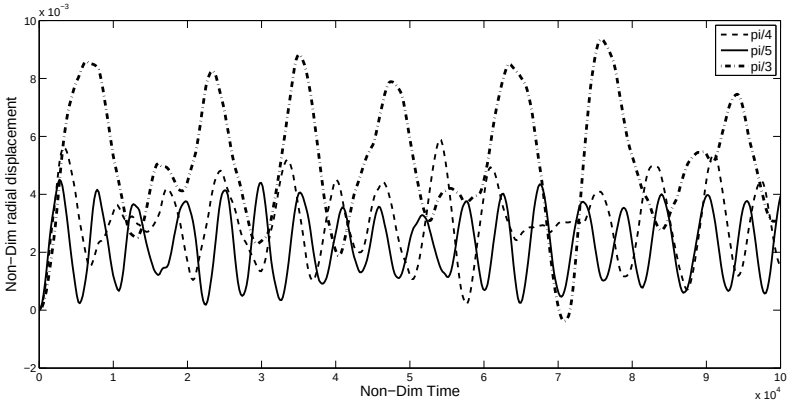

Figure 4 Radial displacement of middle length of the shell versus time for different cone angles.

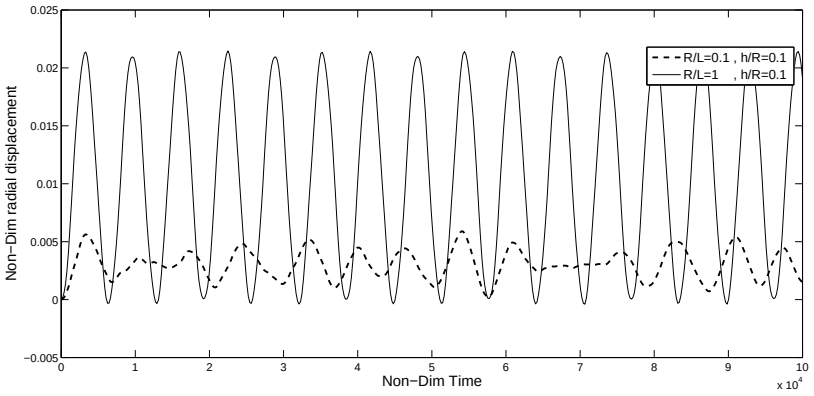

Figure 5 Radial displacement of middle length of the shell versus time.

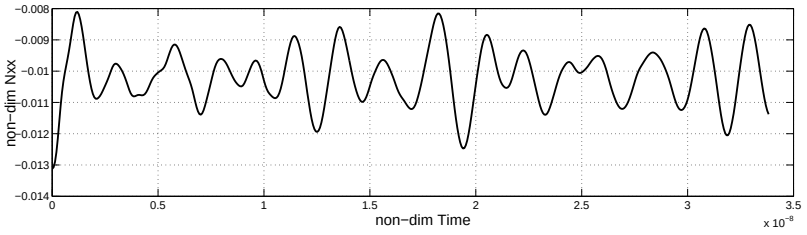

Figure 6 Axial moment of middle length of the shell versus time.

half apex cone angle tend to have larger lateral deflection under internal applied thermal shock loads.

Now, consider a conical shell with similar material and thermal shock load of the previous example. The ratio of thickness to small radius is assumed to be 0.1 and ratio of small radius to length of the conical shell is assumed to be 0.1 and 1. Figure 5 shows the lateral deflection of the shell middle length versus time. This figure shows that, for the same ratio of h/R, when the ratio of small radius to length of conical shell is increased, the lateral deflection is also increased.

Figure 6 shows the axial moment of the shell middle length versus time. Figure 7 shows the axial force of the shell middle length versus time.

Now consider the same type of applied thermal shock load, as given by Eq. (23), but with different amplitudes. The shock amplitude is assumed to be 50, 100, and 200. The plots of thermal shock loads are shown in Fig. 8. Figures 9 and 10 show the lateral deflection and temperature of the shell middle length versus time. When the shock amplitude is increased, the radial middle length deflections of shell versus time and the induced temperatures are increased.

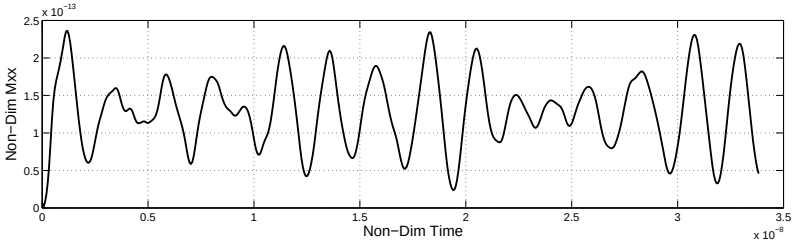

Figure 7 Axial force of middle length of the shell versus time.

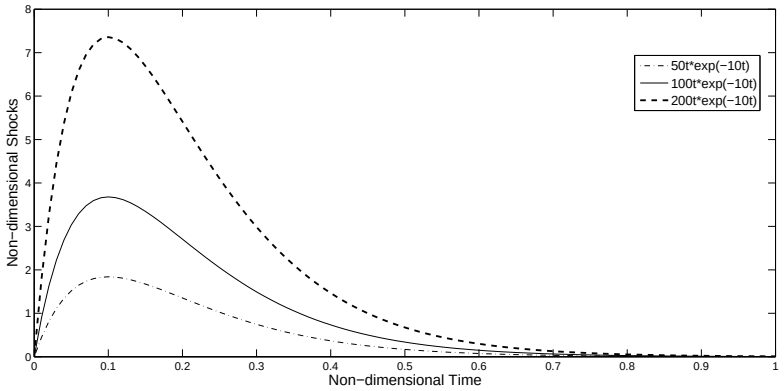

Figure 8 Shocks with different amplitudes

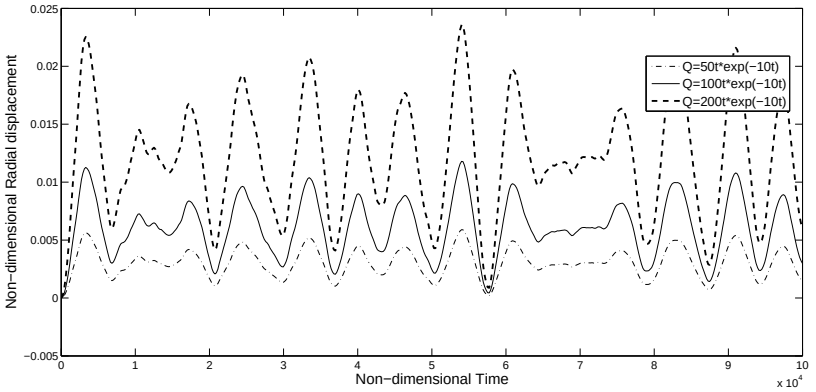

Figure 9 Radial displacement of middle length of shell versus time with shocks.

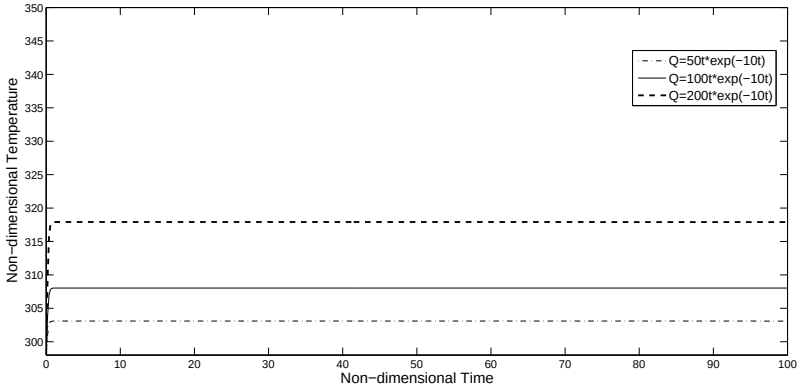

Figure 10 Temperature of middle length and mid-plane of the shell versus time with shocks.

3 Conclusion

Figures 2 to 10 show the behavior of a truncated conical shell made of functionally graded materials under internal thermal shock load. The response of the shell is obtained under the coupled thermoelastic assumption. The figures represent vibratory behavior under such a thermal shock load and the coupled thermoelastic assumption. The question then arises that why wave fronts (in temperature, displacement, and stress fields) are not detected in any of the given figures? Are the wave fronts created and not seen in the figures, or the wave fronts are absent in the shells or plates under thermal shock loads? This is an important question to be carefully addresses.

Referring to Chapters 8 and 9 of reference [21], wave fronts under coupled thermoelastic assumption are observed in different types of structures. The structures discussed in this reference, are analyzed using the theory of thermoelasticity. Plate and shell structures are based on the flexural theory, where the stresses are lumped across the thickness. This assumption results into ignorance of the wave fronts across the plate or shell thickness. That is, while the wave fronts exist across the thickness, but due to the flexural assumption they are not detected. Applying thermal shock loads to the sides of the flexural members result to vibratory behavior, as presented in this article.

Appendix

$$\int \frac{E(z)}{1-\upsilon^2}dz = A_{111} \qquad \int \frac{E(z)}{1-\upsilon^2}zdz = B_{111} \qquad \int \frac{E(z)}{1-\upsilon^2}\upsilon dz = A'_{111}$$
$$\int \frac{E(z)}{1-\upsilon^2}\upsilon z dz = B'_{111} \qquad \int \frac{E(z)}{2(1+\upsilon)}dz = A''_{111} \qquad \int \frac{E(z)}{2(1+\upsilon)}zdz = B''_{111}$$
$$\int \frac{E(z)}{1+\upsilon}dz = A'''_{111} \qquad \int \frac{E(z)}{1+\upsilon}zdz = B'''_{111} \qquad \int \upsilon\frac{E(z)}{1-\upsilon^2}z^2dz = C_{111}$$
$$\int \upsilon\frac{E(z)}{1-\upsilon^2}z^2dz = C'_{111} \qquad \int \frac{E(z).\alpha(z)}{1-\upsilon}dz = G_{11} = H_1$$
$$\int \frac{E(z)}{1+\upsilon}z^2dz = C''''_{111} \qquad \int \frac{E(z).\alpha(z)}{1-\upsilon}zdz = G_{22} = H_2$$
$$\int \frac{E(z).\alpha(z)}{1-\upsilon}z^2dz = G_{33} = H_3 \qquad \int \rho(z).c(z)dz = K_1 \qquad \int k(z)dz = J_1$$
$$\int \rho(z).c(z)zdz = K_2 \qquad \int k(z)zdz = J_2 \qquad \int \rho(z).c(z)z^2dz = K_3$$
$$\int k(z)z^2dz = J_3 \tag{24}$$

References

[1] Ignaczak, J., and Nowacki, W. "Transversal Vibration of a Plate, Produced by Heating", Archiwum Mechaniki Stosowanej, pp. 650-667, (1961).

[2] Jones, J.P., "Thermoelastic Vibrations of a Beam", The Journal of the Acoustical Society of America, Vol. 39, No. 3, pp. 542-548, (1966).

[3] Manoach, E., and Ribeiro, P., "Coupled, Thermoelastic, Large Amplitude Vibrations of Timoshenko Beams", International Journal of Mechanical Sciences, Vol. 46, No. 11, pp. 1589-1606, (2004).

[4] Babaei, M.H., Abbasi, M., and Eslami, M.R., "Coupled Thermoelasticity of Functionally Graded Beams", Journal of Thermal Stresses, Vol. 31(8), pp. 680-697, (2008).

[5] Inan, E., "Coupled Theory of Thermoelastic Plates", Acta Mechanica, Vol. 14, No. 1, pp. 1-29, (1972).

[6] Chang, W.P., and Wan, S.M., "Thermomechanically Coupled Non-linear Vibration of Plates", International Journal of Non-Linear Mechanics, Vol. 21, No. 5, pp. 375-389, (1986).

[7] Trajkovski, D., and Cuki, R., "A Coupled Problem of Thermoelastic Vibrations of a Circular Plate with Exact Boundary Conditions", Mechanics Research Communications, Vol. 26, No. 2, pp. 217-224, (1999).

[8] Yeh, Y.L., "The Effect of Thermo-mechanical Coupling for a Simply Supported Orthotropic Rectangular Plate on Non-linear Dynamics", Thin-Walled Structures, Vol. 43, No. 8, pp. 1277-1295, (2005).

[9] Akbarzadeh, A.H., Abbasi, M., and Eslami, M.R., "Coupled Thermoelasticity of Functionally Graded Plates Based on the Third-order Shear Deformation Theory", Thin-Walled Structures, Vol. 53, pp. 141-155, (2012).

[10] Jafarinezhad, M.R., and Eslami, M.R., "Coupled Thermoelasticity of FGM Annular Plate under Lateral Thermal Shock", Composite Structures, Vol. 168, pp. 758-771, (2017).

[11] McQuillen, E.J., and Brull, M.A., "Dynamic Thermoelastic Response of Cylindrical Shells", Journal of Applied Mechanics, Vol. 37, No. 3, pp. 661-670, (1970).

[12] Eslami, M.R., Shakeri, M., and Sedaghati, R., "Coupled Thermoelasticity of an Axially Symmetric Cylindrical Shell", Journal of Thermal Stresses, Vol. 17, No. 1, pp. 115-135, (1994).

[13] Chang, J.S., and Shyong, J.W., "Thermally Induced Vibration of Laminated Circular Cylindrical Shell Panels", Composites Science and Technology, Vol. 51, No. 3, pp. 419-427, (1994).

[14] Eslami, M.R., Shakeri, M., Ohadi, A.R., and Shiari, B., "Coupled Thermoelasticity of Shells of Revolution: Effect of Normal Stress and Coupling", AIAA Journal, Vol. 37(4), pp. 496-504, (1999).

[15] Bahtui, A., and Eslami M.R., "Coupled Thermoelasticity of Functionally Graded Cylindrical Shells", Mechanics Research Communications, Vol. 34, No. 1, pp. 1-18, (2007).

[16] Kraus, H., "Thermally Induced Vibrations of Thin Nonshallow Spherical Shells", AIAA Journal, Vol. 4, No. 3, pp. 500-505, (1966).

[17] Amiri, M., Bateni, M., and Eslami, M.R, "Dynamic Coupled Thermoelastic Response of Thin Spherical Shells", Journal of Structural Engineering & Applied Mechanics, doi.org/10.31462/jseam.2019.02053062

[18] Soltani, N., Abrinia, K., Ghaderi, P., and Hakimelahi, B., "A Numerical Solution for the Coupled Dynamic Thermoelasticity of Axisymmetric Thin Conical Shells", Mathematical and Computer Modelling, Vol. 55, pp. 608-621, (2012).

[19] Heydarpour, Y., and Aghdam, M.M., "Transient Analysis of Rotating Functionally Graded Truncated Conical Shells Based on the Lord-Shulman Model", Thin-Walled Structures, Vol. 104, pp. 168-184, (2016).

[20] Reddy, J.N. *Theory and Analysis of Elastic Plates and Shells*, CRC Press, 2006.

[21] Hetnarski, R.B. , and Eslami, M.R. *Thermal Stresses: Advanced Theory and Applications*, Second Edition, Springer, Switzerland, 2019.

[22] Bateni, M., and Eslami, M.R., "Thermally Nonlinear Generalized Thermoelasticity of a Layer", Journal of Thermal Stresses, Vol. 40, No. 10, pp. 1320-1338, (2017).

[23] Bateni, M., and Eslami, M.R., "Thermally Nonlinear Generalized Thermoelasticity: A Note on the Thermal Boundary Conditions", Acta Mechanica, Vol. 229, No. 2, pp. 807-826, (2018).

[24] Eslami, M.R. *Finite Elements Methods in Mechanics*, Springer, Switzerland, 2014.

[25] Brancik "The Fast Computing Method of Numerical Inversion of Laplace Transforms Using FFT Algorithm", Proc. of 5th EDS 98 Int. Conf., Brno, Czech Republic., pp. 97-100, (1998).